7.12 RADIATIVE HEATING PROFILES IN THE CONVECTIVE TROPICS: A COMPARISON OF OBSERVATIONS AND MODELS

Sally A. McFarlane*, James H. Mather and Thomas P. Ackerman

Pacific Northwest National Laboratory, Richland, Washington

1. INTRODUCTION

The variability of water vapor and clouds in the atmosphere, and their associated radiative heating, is an important driver of atmospheric circulation. Changes in infrared (IR) cooling due to water vapor variability in the tropics affect the conditional instability for deep convection (Zhang and Chou, 1999). Cirrus anvils destabilize the atmosphere and may induce vertical lifting and turbulence due to cloud base warming and cloud top cooling (Gu and Liou, 2000). Recent studies using idealized simulations (Raymond, 2000) and 2D cloud-resolving models with large horizontal domains (Grabowski and Moncrieff, 2002) have shown that differential radiative heating between clear and cloudy regions can drive large-scale tropical dynamics. To further understand the role of radiative heating on the local scale and for large scale dynamics, observations of radiative heating profiles are required to assess model results.

While we have good knowledge of radiative fluxes at the top-of-atmosphere (TOA) and at specific surface sites, observations of atmospheric profiles of radiative heating, particularly in cloudy conditions, have largely been unavailable. Current estimates of cloudy sky radiative heating in the tropics are based primarily on model simulations (e.g., Fu et al., 1995) or satellite observations (Bergman and Hendon, 1998). The long time series of observations taken at the Department of Energy's Atmospheric Radiation Measurement (ARM) program sites on the islands of Manus (-2.06^o S, 147.43^o E) and Nauru (0.521^o S, 166.92^o E) in the tropical western Pacific (TWP) provides a more direct method of calculating all sky heating rate profiles with high vertical and temporal resolution. The ARM Program has begun a project to compute radiative heating rate profiles routinely at the observational sites at Nauru and Manus, using observed and retrieved profiles of water vapor and condensed water phase, particle size, and mass. These heating rate profiles represent a unique dataset for model comparison.

Recently, a new type of global climate model (GCM), called the Multi-scale Modeling Framework (MMF) has been proposed by Randall and colleagues (Randall et al., 2003; Khairoutdinov and Randall, 2001). The MMF consists of a 2D cloud system resolving model (CSRM) embedded into each column of a GCM, replacing the conventional cloud and radiation parameterizations. Although much more computationally expensive than a typical GCM, the MMF treats cloud dynamics explicitly within the CSRM, which has the potential to improved the representation of cloud processes within a GCM.

This study presents an initial evaluation of the ability of the MMF to reproduce radiative heating rate profiles within the tropics. We compare the retrieved cloud properties and calculated heating rate profiles from the ARM observations to the simulated clouds and heating rates from the MMF and its parent GCM for a month at both Nauru and Manus. At Nauru, we selected the Nauru99 intensive operational period (June 15 – July 15, 1999) because of the increased frequency of radiosonde launches during this period. It also represents one of the most convectively active periods at Nauru during the first few years of ARM observations. The Manus period (February – March 2000) was selected because it corresponds to a period with a transition from convectively suppressed to active conditions.

2. CLOUD MICROPHYSICAL RETRIEVALS AND HEATING RATE CALCULATIONS

Profiles of cloud microphysical properties (phase, mass content, and particle size) are calculated by applying simple retrievals to the ARM millimeter wave radar data. Radar reflectivity (Z) at each height is divided into liquid and ice contributions based on a simple temperature scheme with levels below -16C assumed to contain all ice, levels above 0C assumed to contain all liquid, and other levels assumed to be a linear mixture of ice and water. Liquid water content (LWC) is calculated from LWC = $(N_d Z/3.6)^{1/1.8}$ assuming a number concentration, N_d, of 100 cm^{-3} (Sassen and Liao, 1994). Liquid clouds are assumed to have a log normal size distribution with a width of σ = 0.35, and therefore the mode radius is given by $r_m = \left(\frac{3LWC}{4\pi\rho_w N_d \exp(9\sigma^2)} \right)^{\frac{1}{3}}$, where ρ_w is the density of water (Frisch et al., 1995). For ice clouds, the ice water content (IWC) is calculated from the relationship of Liu and Illingworth (2000), IWC = $(0.097)Z^{0.59}$. Ice effective radius, r_e, is parameterized as a function of temperature, r_e = (75.3 + 0.5895T)/2 (Ivanova et al, 2001). To reduce the time required for radiative transfer calculations, the microphysical properties are calculated every 10 seconds and then averaged to 20 minute intervals. Cloud fraction at each level is also

* *Corresponding author's address:* Sally A. McFarlane, Pacific Northwest National Laboratory, P.O. Box 999, Richland, Washington, 99352, United States; e-mail: Sally.McFarlane@pnl.gov

calculated for the 20 minute interval. Intervals with any occurrence of radar reflectivity greater than 0 dBZ at temperatures above 0C are removed from the dataset since the radar retrievals are not applicable to precipitating clouds.

Broadband fluxes and heating rates are calculated using the spherical harmonics discrete ordinates method (SHDOM) model (Evans 1998) in one-dimensional mode with the correlated k-distributions from the Rapid Radiative Transfer Model (RRTM) (Mlawer et al., 1997). In the SW region (.2-3.85 μm) bulk scattering properties of ice crystals are obtained by integrating the single scattering properties of Yang et al., 2000 over a gamma size distribution. In the LW region (3.85-1000 μm), ice cloud scattering properties are calculated from Mie theory assuming spheres with volume/area ratios equivalent to the volume/area ratios of the crystals used in the SW calculations. Temperature and humidity profiles are interpolated from radiosonde profiles. Water vapor profiles are scaled to the integrated column water vapor measured by a 2-channel microwave radiometer at the ARM site.

For both Manus and Nauru, radiative fluxes and heating rates were calculated at 20-minute intervals throughout the vertical column. Boundary layer clouds tend to be highly variable in time. To minimize the impact of averaging the boundary layer cloud properties, two sets of radiative transfer calculations were done for each site. First, a calculation was done with the 20-minute averaged retrieved cloud properties. Secondly, a calculation was done with only the boundary layer clouds (heights < 2 km) removed. Then the temporal cloud fraction was used to combine the two sets of cloud fluxes into a product that best represents an average over the 20-minute period.

3. MODELS

For this study, the parent GCM of the MMF is the NCAR Community Atmosphere Model (CAM 3.0). This version of the CAM uses the finite volume dynamical core and has 26 vertical layers and horizontal resolution of 2 degrees latitude by 2.5 degrees longitude. The embedded CSRM (Khairoutdinov and Randall, 2003) has 64 columns at 4 km spacing, and 24 layers in the vertical, which coincide with the lowest 24 levels of the CAM. The CSRM domain was aligned in the east-west direction. Time steps are 1 hour for the CAM and 20 seconds for the CSRM. The CSRM replaces all of the cloud and radiation parameterizations within the CAM. We perform two simulations – one with the MMF and one with the CAM run with its standard cloud and radiation parameterization. For this study, we examine output from the CAM grid box nearest to each ARM site. For the MMF results, we examine the average over the 64 CSRM columns within the CAM grid box.

The simulations were started with the month September 1997 using initial model fields from a CAM spinup simulation and observed monthly sea surface temperatures (SST). The simulation has currently run through July 1999. CAM model runs were performed for the same period with the same SST values. Since the MMF simulation has not yet reached the year 2000, for the Manus comparison, we compare the simulated period of February – March, 1999 to the observed period of February – March, 2000. Both of these periods were within a La Nina period that had a relatively weak impact at Manus, therefore we expect the two periods to be climatically similar. Obviously, 2 months of data is not sufficient for a statistically significant comparison. However, even this limited analysis can identify potentially significant areas to be examined more fully in future work.

4. RESULTS

4.1 *Cloud Properties*

Frequency distributions of the condensed water content (CWC = LWC + IWC) at each vertical level are shown in Figure 1 for the observations and models during the Nauru99 period. For this comparison, modeled cloud is defined to be grid boxes with CWC > 1.0e-4 g/m^3, which is the lower detection limit of the radar.

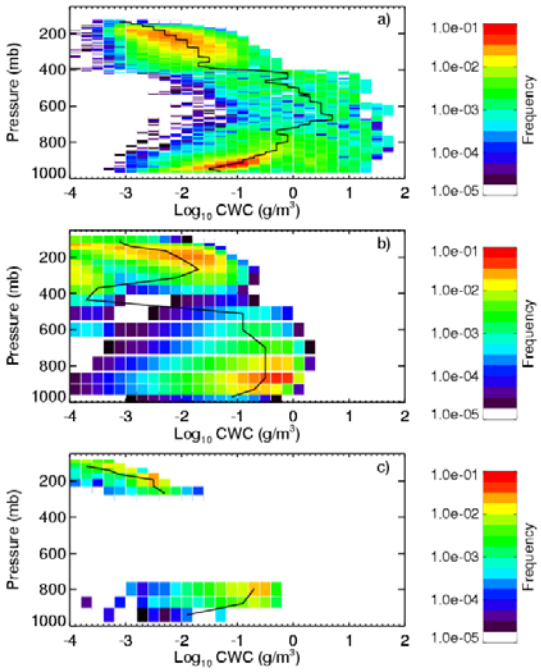

Figure 1. Frequency distribution of CWC for a) ARM radar retrieved clouds, b) MMF clouds and c) CAM clouds for the Nauru99 period. The solid black line indicates the median CWC at each pressure level. The CWC distributions are plotted at the midpoint of each vertical level.

The radar retrievals of CWC reveal a clear vertical structure. In the lowest several kilometers, CWC increases approximately linearly with altitude, which is consistent with diluted adiabatic ascent within shallow cumulus. A second feature, spanning a wide range in

CWC, is found near 500 mb, which corresponds to the freezing level. Above 8 km, CWC decreases with altitude, which likely reflects the settling of larger particles toward the bottom of cirrus layers and less water available at higher altitudes during cirrus formation.

The MMF and CAM both produce the cirrus and shallow cumulus feature, while the MMF also produces some cloudiness around 500-600 mb, near the freezing level. The boundary layer cloud feature is higher in both the CAM and the MMF than it is in the radar observations, which is probably due to the coarse resolution of these models in the lower atmosphere. Additionally, the magnitude of the CWC in the boundary layer cloud region is higher in the MMF and CAM than in the radar retrievals. The cirrus feature in the MMF shows a strong resemblance to the cirrus feature in the radar retrievals, with similar magnitudes of CWC, although the MMF feature is slightly higher. The MMF also has a second cirrus feature at very low values of CWC around 400 mb. We believe this is due to dilution of CWC at cloud base in the CSRM. The cirrus feature in the CAM is much higher and has lower magnitude CWC than the radar retrievals.

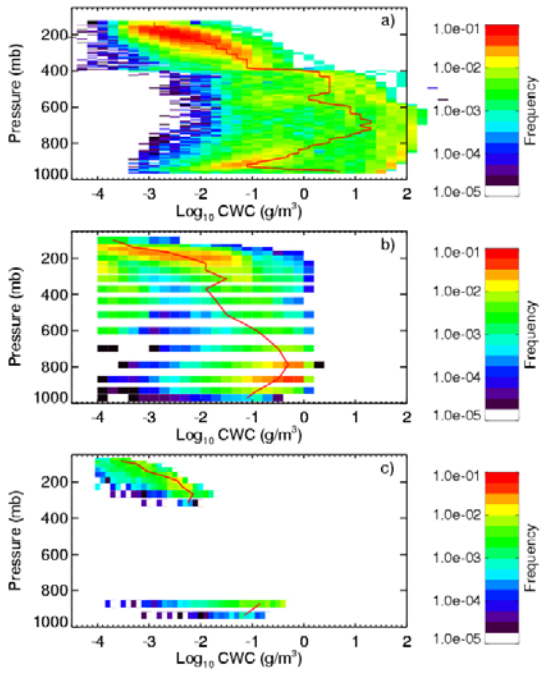

Figure 2. As in Figure 1, but for the Manus observations and simulations.

Figure 2 shows the CWC frequency distributions for the Manus site. The observed frequency of cirrus and mid-level clouds is higher and the frequency of boundary layer clouds is less at Manus than at Nauru. The MMF shows a lower frequency of cirrus and low clouds, but higher frequency of mid-level clouds at Manus. The CAM shows a stronger cirrus feature, but low clouds only exist in 2 model levels at Manus, instead of in 3 levels, as at Nauru.

4.2 *Heating Rates*

Average heating rate profiles for the Nauru99 period are shown in Figure 3. The top row of Figure 3 presents the average clear sky heating rates. The models occasionally retain residual amounts of condensed water, therefore model profiles were classified as clear sky only if they contained no level with CWC > 1.0e-6 g/m3, and the observed profiles were classified as clear sky if there were no significant radar returns within the column (note that the radar might not see very high thin cirrus). Due to the high frequency of fractional cloudiness in the CAM, only 6% of the CAM columns were classified as clear sky, therefore the clear sky heating rate profiles may be statistically noisy. Clear sky represented 40% of the MMF profiles and 16% of the ARM 20 minute averaged profiles.

The clear sky heating rate profiles from the models and calculated from the ARM observations show the same general trends. There is shortwave heating throughout the troposphere, which decreases with altitude as water vapor concentration decreases. In the stratosphere, shortwave heating increases due to ozone. Longwave cooling exists throughout the troposphere, but begins to decrease significantly in the upper troposphere due to the decrease in saturation vapor pressure with decreasing temperature (Hartmann et al., 2001). Near the tropopause, the net longwave effect is heating, due to CO_2 and O_3. The level of zero net radiative heating controls the entry of air into the stratosphere as net heating leads to rising air and net cooling to sinking air (Gettelman et al., 2004).

Although the clear sky profiles are generally similar, there are a few key differences. The level of zero net heating is higher in the MMF and the CAM than in the observed profiles. Gettelman et al. (2004) studied clear sky radiative heating in 5 different radiation models and found that the level of zero net radiative heating varied by ±300 m. Additionally, the modeled and observed heating rates are based on different thermodynamic profiles, which will influence the level of zero net radiative heating. In the ARM heating rate profiles, the longwave cooling begins to decrease in magnitude around 400 mb, while in the model profiles it does not begin decreasing until 300 mb. The MMF clear sky radiative heating profile has a boundary layer feature, with pronounced shortwave heating and longwave cooling that is not present in the other profiles. We restricted the MMF clear sky to cases having CWC = 0.0 throughout the column to rule out any residual condensed water in the model, however, this feature persists and seems to be associated with water vapor in the model. The CAM has a double peak in longwave cooling which is associated with water vapor features in the model. A

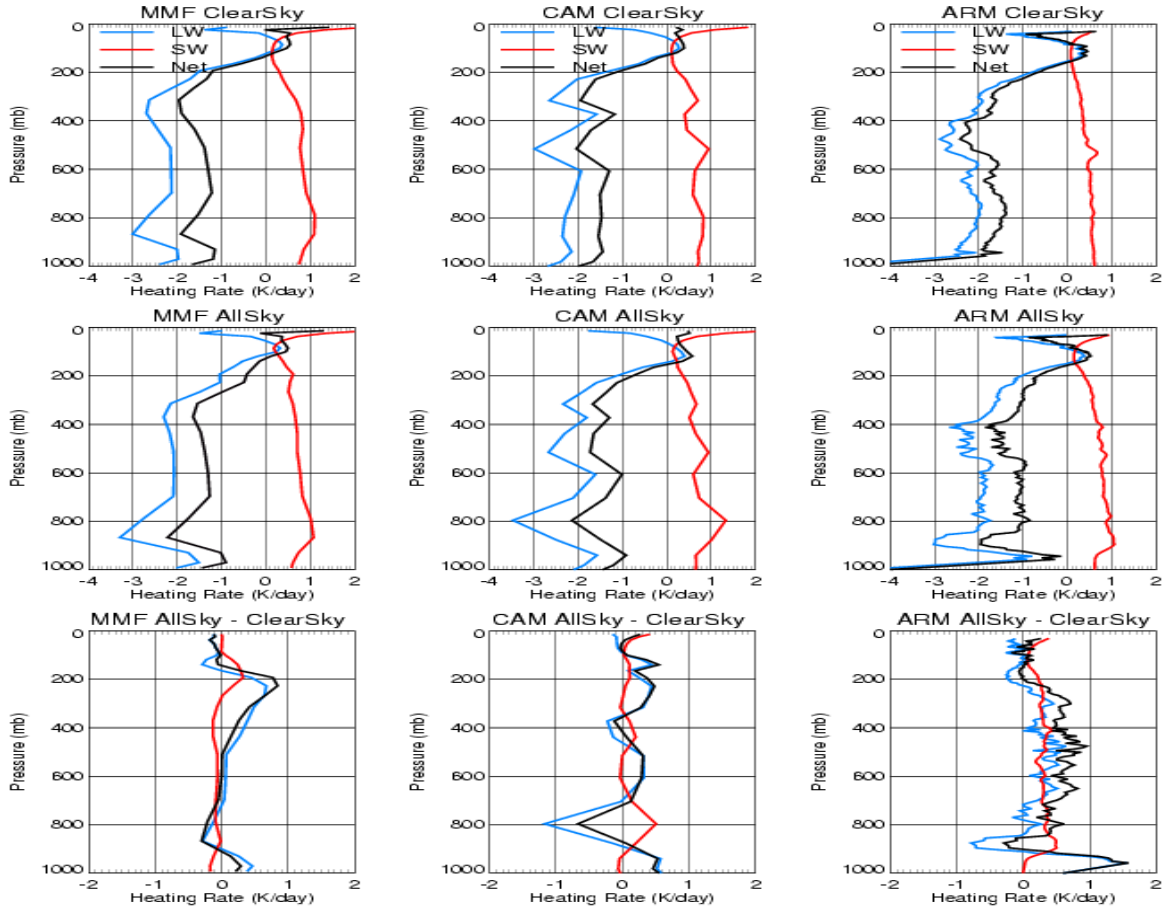

Figure 3. Average heating rates for the Nauru99 period. The clear sky profiles are in the top row, all sky profiles in the second row, and all sky minus clear sky differences in the bottom row.

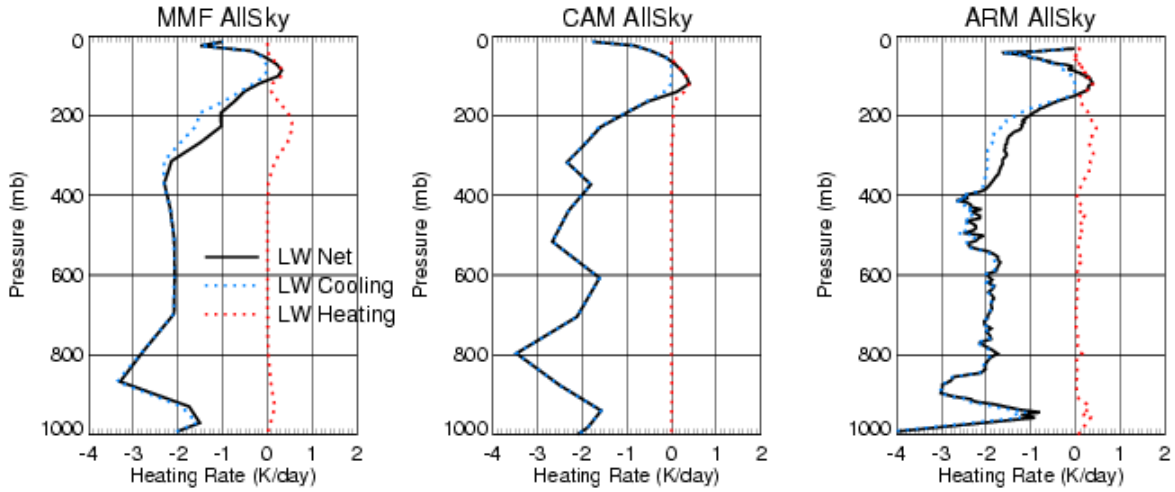

Figure 4. Longwave heating rates for the Nauru99 period, broken down into heating and cooling components. The black line is the net longwave, the blue line is longwave cooling, and the red line is longwave heating.

longer timeseries would allow more clear sky periods, and probably smooth out some of this variability.

The middle row of Figure 3 shows the all-sky average radiative heating rate profiles for the Nauru99 period. Again, the heating rate profiles are generally similar but show some differences. Each profile shows a clear peak in longwave cooling and shortwave heating in the boundary layer. However this feature is higher and broader in the models, which may be due to the low resolution of the models relative to the observations in this region.

In order to isolate the effect of clouds, we examine the difference in the all sky and clear sky heating rate profiles (bottom row of Figure 3). Low cloud causes net cooling in the cloud layer and net warming below the cloud (relative to the clear sky case). The warming below the cloud occurs because the clear sky cooling that would have occurred is greatly reduced. The boundary layer cloud feature in the CAM is too high; the MMF boundary layer cloud feature is closer in altitude to the ARM observations, but the magnitude of the cloud feature is too low because the clear sky cooling at the cloud level is so pronounced. In the mid troposphere, the MMF shows little difference from clear sky while the ARM observations show slight warming throughout. The CAM shows alternately warming and cooling layers from 700 to 400 mb, which is associated with the water vapor features and the limited number of clear sky profiles, as discussed above. The ARM and MMF profiles show net warming, relative to clear sky, in the cirrus layer (200-400 mb) and cooling above. The CAM shows net warming, relative to clear sky, above 400 mb but shows no cooling above.

Because of the few numbers of clear sky points in the CAM, the all sky minus clear sky profiles are noisy. By looking at the longwave heating rate profile alone, we can examine some of the cloud features more clearly. The clear sky troposphere cools in the longwave, due primarily to emission from water vapor. However, in cloudy skies, there is longwave heating in the troposphere as cloud particles absorb infrared radiation. Figure 4 shows the net longwave profile broken down into heating and cooling components. The black line shows the average net longwave profile, the blue line shows the average longwave cooling, and the red line shows the average longwave heating. In the troposphere, both the MMF and ARM profiles show longwave heating features related to boundary layer clouds and cirrus clouds. The ARM profiles also show some longwave heating related to clouds between 400-600 mb. All three profiles show longwave heating in the tropopause layer as ozone absorption becomes important. The CAM profiles show, on average, no longwave heating in the troposphere.

To investigate whether the lack of cloud features in the CAM longwave heating profiles is due to lack of cloud or to the thinness of the cloud that exists, we examine the average cloudiness in the models and observations. In Figure 5, we plot the mean cloud fraction or cloud amount as a function of height. For the CAM, this is simply the mean cloud fraction at each level. For the MMF, each 4 km grid box of the CSRM is either clear or cloudy, so we define cloud amount as the percentage of grid boxes at each level that are cloudy. For the ARM observations, we define two measures of cloud amount. The first measure is the cloud amount that is used in the heating rate calculations, in which boundary layer cloud amount is weighted by the percentage of times cloud was observed during the 20 minute period while clouds above 2 km, when present, are assumed to have 100% cloud amount during the 20 minute period. The second measure is the actual ARM cloud amount, including the percentage of time clouds were observed in the 20 minute period for all levels. We can see that using 100% cloud amount for clouds above 2 km (800 mb) overestimates the amount of cloudiness and might affect the calculated heating rates.

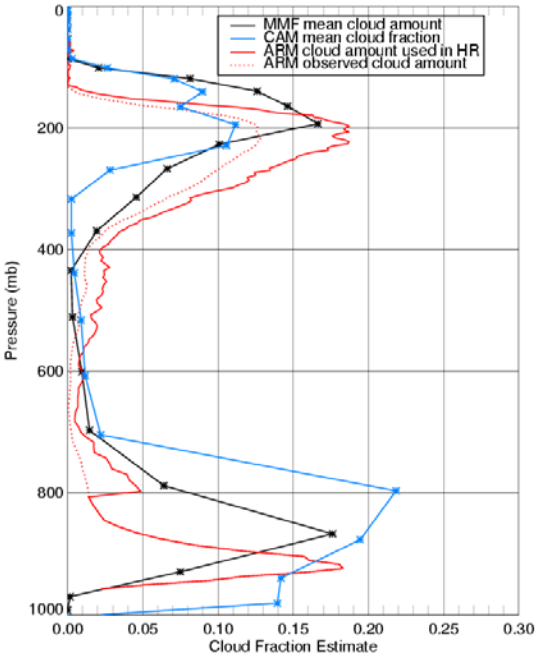

Figure 5. Cloud fraction or amount as a function of height for the Nauru99 period. See text for discussion of the ARM cloud amount.

The models and the observations have remarkably similar cloud amounts. However, as stated previously the boundary layer cloud features in the CAM and MMF are too high and the CAM feature is too broad. Although the CAM has more boundary layer cloud than the MMF and the observations, it has lower average longwave heating because the magnitude of the CWC is lower and because the broad shape of the cloud feature

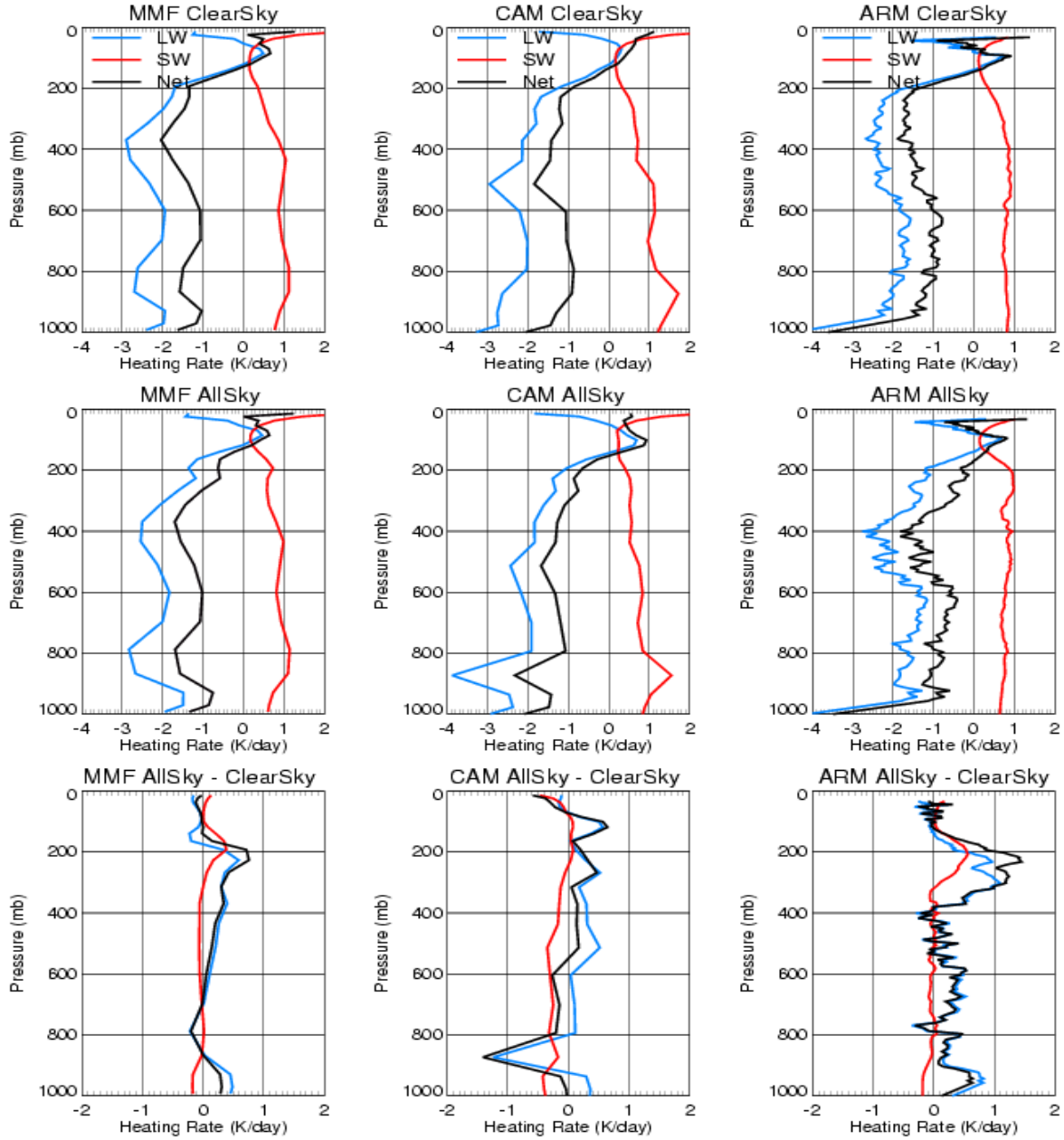

Figure 6. Heating rate profiles. As in Figure 3, but for Manus period

spreads the heating out over several model levels, which reduces the total heating in each level. In the cirrus layer, the CAM has both less cloud amount and lower CWC than the MMF resulting in the negligible cloud signal in the average LW heating profiles.

Figure 6 shows the average heating rate profiles for the Manus period. Although we do not have space to discuss the results in detail, the general trends seen in the Nauru heating rate profiles are also evident in this figure. In the ARM heating rate profiles, the signal due to the boundary layer clouds is weaker and that due to cirrus is higher, representing the increased frequency of cirrus and decreased frequency of boundary layer clouds observed at Manus. The models do not reflect this trend; in fact the CAM has a stronger boundary layer cloud signal at Manus and the MMF heating rate profiles seem basically unchanged

5. CONCLUSIONS

Using the ARM cloud observations at Manus and Nauru, which provide a basis for calculating vertical heating profiles with high vertical and spatial resolution in cloudy skies, we have begun a project to assess the vertical heating rates produced in large scale models. In this initial analysis, we have compared cloud retrievals and calculated heating from one month at each Nauru and Manus to simulated clouds and heating rates from the CAM and MMF models. Preliminary results indicate that the MMF does a better job of reproducing the longwave heating due to cirrus clouds than the CAM. However, the MMF seems to overestimate the shortwave cooling due to clear sky.

Some of the differences in the ARM and model heating rates, particularly in the boundary layer clouds, seem related to the coarse vertical resolution in the models. In future work, we will investigate averaging the ARM observations to the CAM/MMF vertical resolution before calculating the heating rates. We will also examine the difference in the radiative parameterizations used in the CAM/MMF and the radiative transfer model used in the ARM calculations, with specific attention to the clear sky cooling seen in the MMF. Finally, we will expand the comparison to include a much longer time series and more models, including forecast models such as the European Centre for Medium Range Weather Forecasting (ECMWF) model.

A*cknowledgements.* Support for this research was provided by the Computational Sciences and Engineering Initiative as part of the Laboratory Directed Research and Development Program at the Pacific Northwest National Laboratory. Computer time was made available through a Grand Challenge grant from the Molecular Science Computing Facility.

6. REFERENCES

Bergman, J.W. and H.H. Hendon, 1998: Calculating monthly radiative fluxes and heating rates from monthly cloud observations. *J. Atmos. Sci.,* **55,** 3471-3491.

Evans, K.F., 1998: The spherical harmonics discrete ordinates method for three-dimensional atmospheric radiative transfer. *J. Atmos. Sci.,* **55,** 429-446.

Fu, Q., S.K. Kreuger, and K.N. Lious, 1995: Interactions of radiation and convection in simulated tropical cloud clusters. *J. Atmos. Sci.,* **52,** 1310-1328.

Gettelman, A., P. M. de F. Forster, M. Fujiwara, Q. Fu, H. Vomel, L. Gohar, C. Johanson, and M. Ammerman, 2004: Radiation balance of the tropical tropopause layer. *J. Geophys. Res.,* **109,** doi:10.1029/2003JD004190.

Grabowski, W. W. and M.W. Moncrieff, 2002: Large-scale organization of tropical convection in two-dimensional explicit numerical simulations: Effects of interactive radiation. *Quart. Journal Royal Met. Soc.,* **128,** 2349-2375.

Gu, Y. and K.N. Liou, 2000: Interactions of radiation, microphysics, and turbulence in the evolution of cirrus clouds. *J. Atmos. Sci.,* **57,** 2463-2479.

Hartmann, D. L., J.R. Holton, and Q. Fu, 2001: The heat balance of the tropical tropopause, cirrus, and stratospheric dehydration. *Geophys. Res. Letters,* **28,** 1969-1972.

Khairoutdinov, M.F., and D.A. Randall, 2001: A cloud resolving model as a cloudparameterization in the NCAR Community Climate System Model: Preliminary results. *Geophys. Res. Let.,* **28,** 3617-3620.

Khairoutdinov, M.F., and D.A. Randall, 2003: Cloud resolving modeling of the ARM Summer 1997 IOP: Model formulation, results, uncertainties, and sensitivities. *J. Atmos. Sci.,* **60,** 607-625.

Liu, C.L., and A.J. Illingworth, 1999: Toward more accurate retrievals of ice water content from radar measurements of clouds. *J. Appl. Meteor.*, **39**, 1130-1146.

Mlawer, E.J., S.J. Taubman, P.D. Brown, M.J. Iacono and S.A. Clough, 1997: RRTM, a validated correlated-k model for the longwave. *J. Geophys. Res.*, **102,** 16,663-16,682.

Randall, D., M. Khairoutdinov, A. Arakawa, and W. Grabowski, 2003: Breaking the cloud parameterization deadlock. *Bull. Amer. Meteor. Soc., **84,** 1547-1564.*

Raymond, D. J., 2000: The Hadley circulation as a radiative-convective instability. *J. Atmos. Sci.,* **57,** 1286-1297.

Yang, P., K.N. Liou, K. Wyser, and D. Mitchell, 2000: Parameterization of the scattering and absorption properties of individual ice crystals. *J. Geophys. Res.*, **105,** 4699-4718.

Zhang, C. and M.-D. Chou, 1999: Variability of water vapor, infrared radiative cooling, and atmosphereic instability for deep convection in the equatorial western Pacific. *J. Geophys. Res.,* **56,** 711-723.